analytical chemistry

pubs.acs.org/ac Article

High-Throughput Functional Screening of Antigen-Specific T Cells Based on Droplet Microfluidics at a Single-Cell Level

Shiyu Wang,[††] Yang Liu,[††] Yijian Li, Menghua Lv, Kai Gao, Ying He, Wenbo Wei, Yonggang Zhu, Xuan Dong, Xun Xu, Zida Li,* Longqi Liu,* and Ya Liu*

Cite This: https://doi.org/10.1021/acs.analchem.1c03678 Read Online

ACCESS | Metrics & More | Article Recommendations | Supporting Information

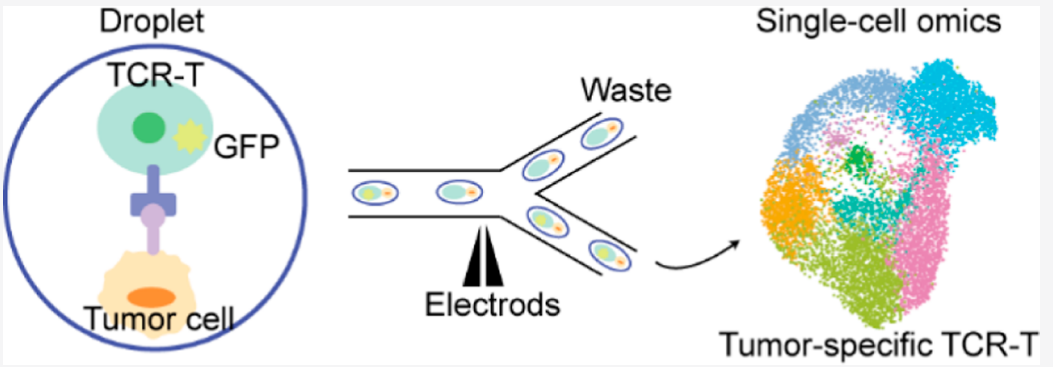

ABSTRACT: The lack of an efficient method for the identification of tumor antigen-specific T cell receptors (TCRs) impedes the development of T cell-based cancer immunotherapies. Here, we introduce a droplet-based microfluidic platform for function-based screening and sorting of tumor antigen-specific T cells with high throughput. We built a reporter cell line by co-transducing the TCR library and reporter genes at the downstream of TCR signaling, and reporter cells fluoresced upon functionally binding with antigens. We co-encapsulated reporter cells and antigen-presenting cells in droplets to allow for stimulation on a single-cell level. Functioning reporter cells specific against the antigen were identified in the microfluidic channel based on the fluorescent signals of the droplets, which were immediately sorted out using dielectrophoresis. We validated the reporter system and sorting results using flow cytometry. We then performed single-cell RNA sequencing on the sorted cells to further validate this platform and demonstrate the compatibility with genetic characterizations. Our platform provides a means for precise and efficient T cell immunotherapy, and the droplet-based high-throughput TCR screening method could potentially facilitate immunotherapeutic screening and promote T cell-based anti-tumor therapies.

INTRODUCTION

Cancer immunotherapy is one of the most promising cancer therapies.[1] T cell-based adoptive cell therapies (T-ACTs), including tumor-infiltrating lymphocyte (TIL) therapy,[2−4] chimeric antigen receptor (CAR)-T therapy, and transgenic T cell receptor (TCR)-T therapy,[5−7] have been shown to regress tumor. TIL therapy was the first T-ACT with demonstrated efficacy, but isolating tumor-reactive TILs from primary tissues remains challenging. CAR-T and TCR-T eliminate the limitation by transducing a receptor with a known specificity to tumor antigens. CAR-T therapies targeting surface markers have achieved great successes in treating B lymphocytic leukemia.[8,9] However, for solid tumor, strong off-target risks hinder CAR-T therapy because surface markers are similarly expressed by adjacent cells.[10] Recently, concerns on neoantigens (epitopes generated by genetic mutations in tumor cells) are raised because normal tissues do not express neoantigens and TCRs targeting them may reduce off-target effects of ACTs. Neoantigens need a presentation by the major histocompatibility complex (MHC), and only TCR-T can recognize them.[5,11,12] However, a hurdle for TCR-T is to define enough neoantigen-specific TCR clonotypes for clinical use because of the enormous diversity of neoantigens across individuals.

Identifying antigen-specific TCRs is not a trivial task given the enormous diversity of TCRs and complicated TCR signaling networks. It is estimated that over 10^6 TCR clonotypes[13] exist in an individual and only a small portion with proper binding affinity to peptide-MHC (pMHC) can

Received: August 26, 2021
Accepted: November 21, 2021

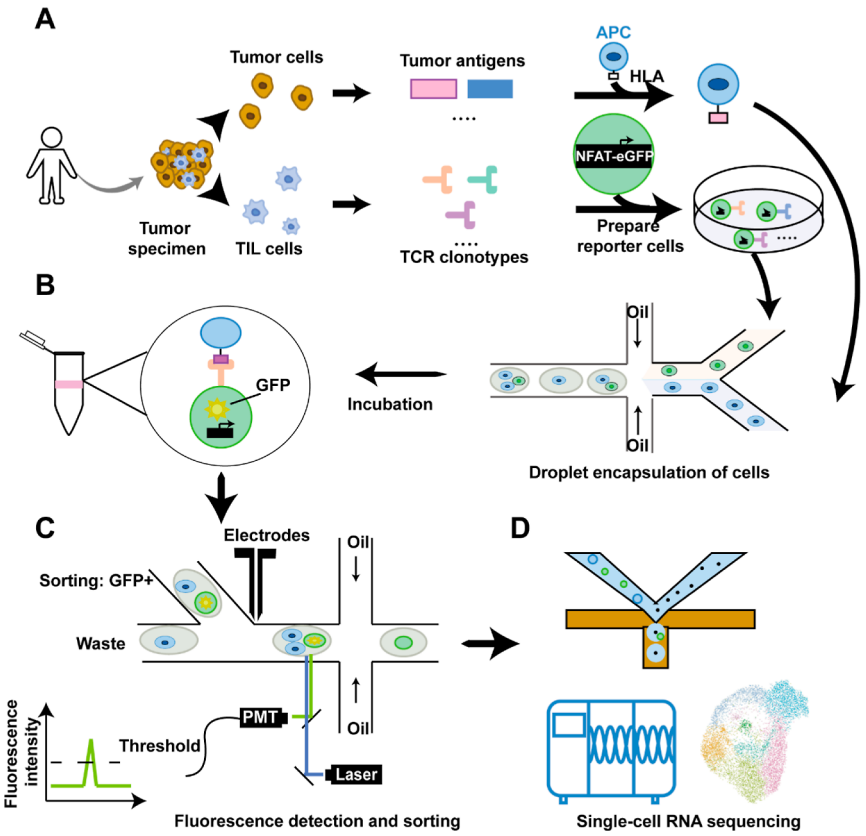

Figure 1. Flowchart of the tumor antigen-specific TCR screening platform. (A) Preparation of TCR-T cells and APCs. Tumor specimen is disassociated, and tumor cells and TIL cells are isolated, respectively. Tumor antigens and tumor-specific TCR clonotypes were predicted from data of TCR sequencing, whole exon sequencing, and mass spectrometry on tumor specimens. Then, TCR clonotypes were transduced into the reporter cell line, and the tumor peptide was loaded on HLA of APCs. (B) Co-encapsulation of cells in droplets. (C) Fluorescence-activated droplets screening and sorting. (D) scRNA-seq of TCR-T cells recovered from sorted droplets.

activate T cells. Furthermore, affinity might not be a reliable indicator of T cell response,[14] and factors such as TCR-pMHC avidity, co-receptor signaling,[15] and a force, so-called "catch bound", in TCR-pMHC interaction[16] are related with high affinity but non-stimulatory interaction.

Up to now, the most common strategy for screening antigen-specific TCRs is pMHC multimers.[17−19] Methods by labeling antigens with fluorophores[20] and DNA barcodes[17,21] can detect 63 ∼ 10^{10} different T-cell specificities simultaneously. However, inefficient production, suboptimal library size, and pMHC multimer instability[22] hinder the practical usage of DNA-barcoded pMHC multimers. Importantly, studies using the multimer-based strategy have rarely examined cellular responses and therefore overlook TCR biological functions. Instead, setting a reporter at the downstream of the TCR signaling pathway can potentially solve the problem. In this strategy, CD3 transmits the TCR-triggered signal through immunoreceptor tyrosine-based activation motifs, recruits PTK zeta chains of TCR-associated protein 70 (ZAP-70) to activate the TCR complex, and then activates IP_3 to let endoplasmic reticulum release Ca^{2+}. Ca^{2+} influx drives nuclear factor of activated T cells (NFAT) to bind response elements at the upstream of the promoter and then to initiate fluorophore protein expression.[23−25] Traditionally, this strategy is performed in plates and only used to verify the antigen-specific TCRs found by the pMHC multimers strategy, given its low throughput.[26] The bulk assays also raise TCR-T unspecific activation risks.[27] To achieve a single-cell resolution, a method was developed to monitor the kinetics of TCR−pMHC recognition in live cells within droplets using a NFAT−eGFP reporter.[28] Because the Ca^{2+}/calcineurin/NFAT network at TCR downstream is prominent in regulating cytotoxicity of cytotoxic lymphocytes,[29] this method can partly reflect response kinetics of single-T cell function to tumor antigens. Nevertheless, 30 min for sorting a single droplet makes the droplet-based method unsuitable for high-throughput scenario.

Here, we developed a droplet-based high-throughput platform for screening and sorting of tumor antigen-specific TCRs with well-defined biological functions. A reporter cell line was generated to express TCRs and green fluorescence protein (GFP) under the regulation of TCR-NFAT signaling (termed "TCR-expressing T cell", TCR-T), and antigen was presented by a cell line with MHC (termed antigen-presenting cell, APC) (Figure 1A). By encapsulating a single TCR-T and APC(s) in the same droplets, single TCR-T cell was stimulated by APC(s) (Figure 1B). After a short incubation, TCR-T cells with expected activities were sorted out using dielectrophoresis based on their fluorescence intensity in droplets (Figure 1C). Both the number and viability of the sorted cells met the requirement of single-cell RNA sequencing (scRNA-seq), and it allowed to visualize the transcriptome especially skewed by TCR stimulation and unveiled antigen-specific TCR clonotypes further (Figure 1D). This platform enabled high-throughput screening (∼450 droplets per second) of functional TCR-pMHC interactions at a single-cell level, providing a

https://doi.org/10.1021/acs.analchem.1c03678
Anal. Chem. XXXX, XXX, XXX−XXX

powerful tool for tumor antigen-specific TCR identification and potentially promoting tumor immunotherapy.

MATERIALS AND METHODS

Reagents. Table S1 of Supporting Information provides a full list of reagents.

Chip Fabrication. Two different microfluidic chips are presented in our work, namely, the droplet generating chip (chip I) and the droplet sorting chip (chip II). In brief, the master molds were fabricated using SU-8 photolithography on 4-inch silicon wafers, and chips were fabricated using polydimethylsiloxane (PDMS). Chip I was bonded on a PDMS-fabricated substrate, and chip II was bonded on a glass slide, using oxygen plasma (Harrick plasma cleaner, PDC-002). The detailed processes of fabricating chips can be found in Supporting Information

Cell Culture. A T2 cell line expressing HLA*A-0201 was used as APCs, and Jurkat cells transduced with DMF5-TCR and NFAT-eGFP reporter genes were employed as TCR-T cells. APCs presented the LAGIGILTV peptide (MART-1_{27-35}) to stimulate TCR-T, which then expressed GFP to characterize the functional recognition of TCRs and antigens.

Fluorescence-Activated Cell Sorting. The activation of TCR-T was determined by fluorescence-activated cell sorting (FACS), and APCs were stained using CellTrace Violet or anti-CD8 antibodies, before encapsulation, to separate APCs from TCR-T (the detailed staining and FACS processes are shown in the Supporting Information).

Statistics of the Cell Distribution in Droplets. TCR-T cells and APCs were labeled with CellTracker CMFDA and CellTrace Violet, respectively. Droplets were generated as the instruction of chip operation in Results, and then, the cell distribution in droplets was examined by fluorescence microscopy. The detailed method for calculating the cell distribution is listed in the Supporting Information.

Cell Viability. AO/PI staining solution was added to cell suspension for counting the percentage of cell viability (Figure S7). Fluorescent pictures were acquired and then analyzed using ImageJ software.

Droplet Sorting. An in-house instrument for fluorescence-activated droplets sorting was developed in this study. The GFP in droplets was activated to emit fluorescence, which was then received and processed by our system. The detailed processes of this system have been shown in the Supporting Information.

Single-Cell RNA-Seq. A DNBelab C4 system was utilized as previously described[30] for single-cell RNA-seq library preparation. The detailed method of data processing, unsupervised clustering, and differential expressed gene (DEG) analysis can be found in the Supporting Information.

Statistical Analysis. Statistical analysis was performed using R (version 4.0.0). Wilcoxon rank-sum test and Student's *t*-test were used in this study. *$p < 0.05$, **$p < 0.01$, and ***$p < 0.001$.

DATA AVAILABILITY

The data that support the findings of this study have been deposited into CNGB Sequence Archive (CNSA)[31] of China National GeneBank DataBase (CNGBdb)[32] with accession number CNP0001907.

RESULTS AND DISCUSSION

Device Design and Operation. We designed two microfluidic chips, namely, the droplet-generating chip (chip I) and droplet-sorting chip (chip II) in this study. As shown in Figure S1A, chip I consisted of two sample inlets, one oil inlet, and one droplet outlet, where negative pressure was applied to drive the flow. Both sample inlets had a radius of 2 mm and a height of 10 mm, supporting a maximum reservoir volume of 125 μL. Oil inlet, with a radius of 3.5 mm and a height of 10 mm, upheld a capacity of 385 μL, which was sufficient for the droplet generation in our experiments. The droplet outlet was connected to a 2 mL collection tube before reaching out to a negative pressure source.

The negative pressure was supplied using a 30 mL syringe assembled with a 3D-printed syringe puller. Negative pressure-based droplet generation ensured a low sample consumption and avoided the issues with bead/cell sedimentation before device entrance. Up to a million droplets could be generated within 10 min (Figure S1B). The negative pressure showed little fluctuation throughout the entire experiment as examined with a pressure sensor connected to the device (Figure S2A). To assess the uniformity of the generated droplets, we aliquoted 10 μL of sample to cover glass, randomly imaged four fields, and analyzed with ImageJ. Results showed that the coefficient of variation was 5% of the diameter (Figure S2B).

To evaluate the effect of cell concentrations on droplet encapsulation, TCR-T and APCs, labeled with CellTrace Violet dye and CellTracker CMFDA dye, respectively, were loaded to the chip I, and results were in good agreement with the theoretical double Poisson distribution, as shown in Figure S3. 50 μL of TCR-T cell suspension (4×10^6/mL), 50 μL of APC suspension (2×10^7/mL), and 150 μL of droplet-generating oil were finally chosen for following tests. As for droplet sorting, we used fluorescence for cell identification and dielectrophoresis for droplet diverting, as shown in Figure S1C. Two independent syringe pumps were applied to control the rate of droplet flow and the distance between two neighboring droplets. Inlet flows were adjusted to sort droplets at 450 droplets per second, and typical parameters for sorting were 80 and 800 μL/h for flow rates of emulsions and spacing oil, respectively, 20 kHz and 2 ms for the frequency and duration of the sorting pulse, respectively, and 1 kV pp for the peak-to-peak voltage applied across electrodes.

Cellular Reporter System. Edited Jurkat cells and T2 cells formed a reporter system: Jurkat cells were transduced with genes to constitutively express TCRs and conditionally express fluorescent protein under the regulation of NFAT, and T2 cells expressing the MHC bound peptides to form a peptide-MHC complex (pMHC) (Figure S4). When the TCR recognized the pMHC, TCR-triggered signaling initiated GFP expression (the pathway is shown in Introduction). Wild-type T2 cells express the human leukocyte antigen-A*0201 (HLA-A*0201, the human version of MHC) receptor and co-stimulatory molecules but not TAP and HLA-II. The lack of TAP makes T2 cells unable to load intracellular peptides on HLA, and functional loss of HLA-II avoids the intervention of HLA class II antigens. Additionally, it is possible to edit T2 with other HLA-I molecules other than HLA-A*0201. Jurkat is a T lymphoblast equipped with similar phenotypes and intracellular signaling transductions as primary T cells. Therefore, T2 and Jurkat were chosen in this study. To demonstrate the effectivity and specificity of the reporter system, DMF5, a TCR

https://doi.org/10.1021/acs.analchem.1c03678
Anal. Chem. XXXX, XXX, XXX−XXX

clonotype targeting MART-1_{27-35} protein, was employed to generate "TCR-T" cells. In order to enhance the transduced TCR expression, we replaced the constant region of transduced TCR with a murine-derived sequence[33] and over-expressed CD8 in reporter cells to strengthen co-stimulatory signaling.[34] Following overnight incubation, the peptide was loaded on the HLA to form the pMHC.

To validate the reporter system performance, we stimulated TCR-T with a mixture of anti-CD3 and anti-CD28 antibodies and APCs loaded with MART-1_{27-35} peptide, separately. After the stimulation with anti-CD3 and anti-CD28 antibodies, both the percentage of GFP$^+$ TCR-T cells (Figure S5) and mean fluorescence intensity (MFI, Figure S5) increased significantly after 3 h, and these values increased consistently in the first 12 h and reached a peak in the next 12 h, suggesting that the downstream signaling pathway of CD3 could be activated effectively. After that, we examined the response kinetics of TCR-T cells with different numbers of APCs and various concentrations of peptide stimulation. Results showed that TCR-T activation in bulk assay depended on the concentration (2.5 μg/mL−80 μg/mL) of peptides treating APCs, and the control group which was not loaded with APCs with the MART-1_{27-35} peptide was not activated, as shown in Figure 2A,B. Additionally, the growth of GFP$^+$ cell percentage was no longer significant when the peptide concentration was up to 80 μg/mL and the TCR-T/APC ratio was 1:3. Unlike bulk assays, cell incubation inside the droplet was highly influenced by the droplet volume.[29] As such, we monitored cell viability in droplets over a period of 12 h. Results showed that the value was higher than 75% within first 8 h before declining to almost 50% at 12 h (Figure S7). Combined together, these results suggest that it is proper to stimulate TCR-T cells with peptide-loaded APCs for 6 h to increase cell viability.

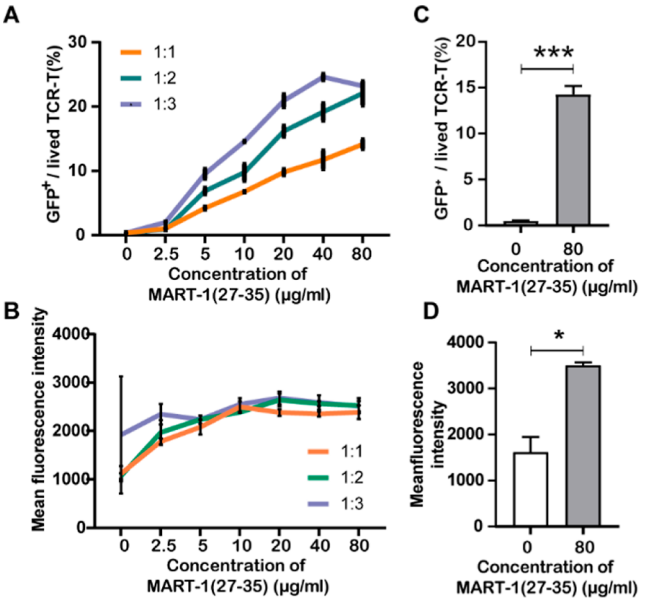

Figure 2. GFP expression of TCR-T cells stimulated by pMHC. (A) Percentage of GFP$^+$ TCR-T cells stimulated by APCs treated with 0, 2.5, 5, 10, 20, and 40 μg/mL peptide at different TCR-T: APC ratios (1:1, 1:2, and 1:3) in a plate. (B) Mean fluorescence intensity (MFI) of GFP$^+$ TCR-T cells stimulated by APCs treated with 0, 2.5, 5, 10, 20, 40, 80, and 160 μg/mL peptide at different TCR-T: APC ratios (1:1, 1:2, and 1:3) in a plate. Two-way ANOVA test examines the difference between groups, and Tukey's multiple comparison examines the difference between samples. (C) Viability of cells in droplets after being cultured for different time durations. (D) Percentage of GFP$^+$ TCR-T cells stimulated by APC(s) treated with 80 μg/mL peptide in droplets. (E) MFI of GFP$^+$ TCR-T cells stimulated by APC(s) treated with 80 μg/mL peptide in droplets. For (C), (D), and (E), Wilcox-ranked test is used to examine differences. *p < 0.05, **p < 0.01, ***p < 0.001, and ns p> 0.05.

We compartmented one TCR-T cell with APC(s) in droplets to investigate cell activation at a single-cell level. APCs were pre-treated with 10, 20, 40, and 80 μg/mL peptide solution (Figures 2C,D and S8). After 6 h of culture, TCR-T expressed GFP in a peptide dose-dependent manner. Considering that 17.9% TCR-T could be encapsulated with APC(s) on average and about 13% of TCR-T cells were activated by APCs treated with 80 μg/mL peptide solution, 6 h stimulation achieved an activation efficiency of about 72% (Figure S3).

It was also reported that 70−75% of cells could be activated[28,35] by either unspecific or pMHC stimulation. Heterogeneity and cellular status of T cells and the loss of the transgene expression following recombination events in the genome might be responsible for the failed GFP expression in about 25−30% TCR-T cells. As indicated by Segaliny et al.,[28] increasing the ratio of APCs to TCR-T could increase the probability of TCR-T−APC contact and thus increase the percentage of GFP$^+$ cells. Another possible reason is that cross-linking of multiple TCR molecules on one T cell leads to stronger intracellular signaling and consequently stronger eGFP expression. However, Segaliny et al. detected the GFP fluorescence of bulk TCR-T cells using a plate reader, from which the signal per cell cannot be examined. We conducted flow cytometry and showed that MFI of GFP$^+$ TCR-T cells was not significantly increased with the increased APC-to-TCR-T ratio. Therefore, the increased possibility of APC−TCR-T interaction with a higher APC number should be the main factor to affect TCR-T activation in bulk assays. In droplets, our results suggested that factors affecting cell activation were different from the bulk system. According to the cell distribution in droplets, TCR-T could contact one or two APCs, indicating that the cell number may not be the primary factor affecting T cell activation in droplets. Instead, we found that increasing peptide concentration for APC treatment enhanced the GFP expression of TCR-T cells, suggesting that interaction between TCR-T and APCs determined the GFP expression of TCR-T cells in droplets. Because T2 is TAP-deficient, it shows lower MHC expression on the cell surface and upregulates MHC expression when being treated with antigen peptides, which in turn promotes the cross-linking of TCRs and enhances GFP expression. In the study, this mechanism could also explain the observation that APCs treated with a higher dose of peptides favored GFP expression in droplets. Thus, experiments of TCR-T activation in droplets could reflect the function of single TCR-T, which was masked in bulk assays.

Sorting GFP$^+$ TCR-T Cells. Functional TCR-T cells, which expressed GFP signals upon binding to the peptide−MHC complex, were sorted for downstream analysis based on the fluorescence intensity. The simultaneous appearance of photo-multiplier tube (PMT), comparator, and single-chip micro-computer (SMC) pulses (Figure 3A) indicate that a positive droplet is found and sorted. A comparator is used to define whether a signal transferred from the PMT represents a positive droplet (GFP$^+$) that appeared. If a comparator detects

https://doi.org/10.1021/acs.analchem.1c03678
Anal. Chem. XXXX, XXX, XXX−XXX

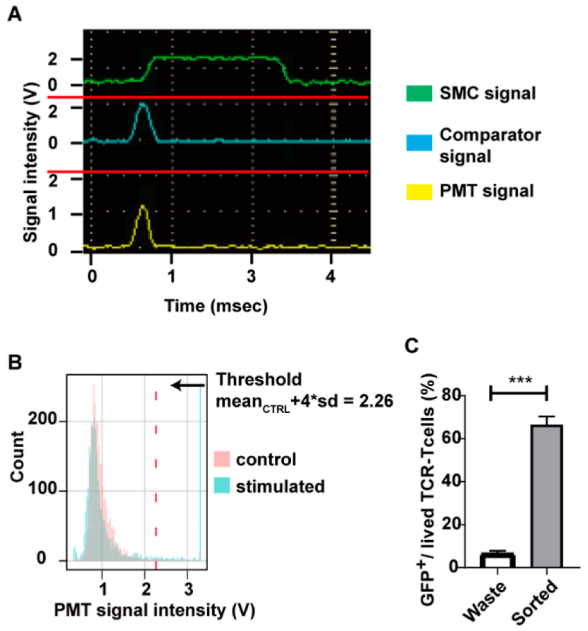

Figure 3. Phenotypic screening and sorting of GFP-positive cells. (A) Representative time traces recorded for a positive droplet detected by the PMT, comparator, and SMC. (B) Signal distribution of control and stimulated droplets. Mean + 4*standard s.d. of signals of control samples set as a threshold for sorting droplets. (C) Percentage of GFP$^+$ TCR-T cells in either sorted and wasted droplets were measured by flow cytometry. The *y*-axis indicates the true positive rate of TCR-T in sorted droplets and false negative rate in waste. Wilcox-ranked test is used. ***$P < 0.001$. PMT, photo-multiplier tube. SMC, single-chip microcomputer.

the signal, it will transfer a signal to trigger SMC to record the signal of the PMT. If the max value of the signal is above the threshold, the SMC will trigger the wave generator to produce a 20 kHz, 2 ms pulse which is then augmented to 1 kV pp. With the pulse, the droplet will be sorted by dielectrophoresis. In order to determine the sorting threshold, droplets encapsulated with TCR-T cells and untreated APCs were used as negative controls, and the fluorescence signals were recorded as baseline signals. Signals of droplets encapsulated with peptide-treated APCs were regarded as positive signals. According to the relative amplitudes of these signals, we adopted the mean of negative signals plus four standard deviations (s.d.) as the threshold, as shown in Figure 3B. Droplets were sorted at a frequency of 450/s, and the sorted cells recovered from droplets were validated by flow cytometry. As shown in Figure 3C, about 70% of the TCR-T cells sorted out were GFP$^+$, while only 4% of the discarded cells were GFP$^+$. The relatively high true positive rate of the sorting device suggested an effective enrichment (enrichment factor = 4.43 ± 0.21) of GFP-positive cells in our system. Nevertheless, further improvement might be necessary to increase the performance of the platform. Like other sorting systems such as FACS, the inconsistent signal intensity is the primary factor affecting the sorting performance. As shown in Figure S5, the expression level of GFP was not consistent for all TCR-T cells, suggesting that finding a clear cut method for the detection of threshold was not practical. By raising the gating threshold, we could decrease the false positive rate, with the tradeoff of increased loss of target cells (false negative). Alternatively, because GFP expression is limited by cell capacity, replacing GFP with a responsive reporter system could potentially improve sorting performance.[36] For example, cascade reactions, such as ones using luciferase as reporters, can break through the limitation of intracellular expression and generate brighter fluorescence. Indeed, the NFAT-luciferase system has been used to report TCR-T cell activation.[24,37,38] Another factor that could have compromised the sensitivity and specificity of the sorting is the inconsistent locations of cells

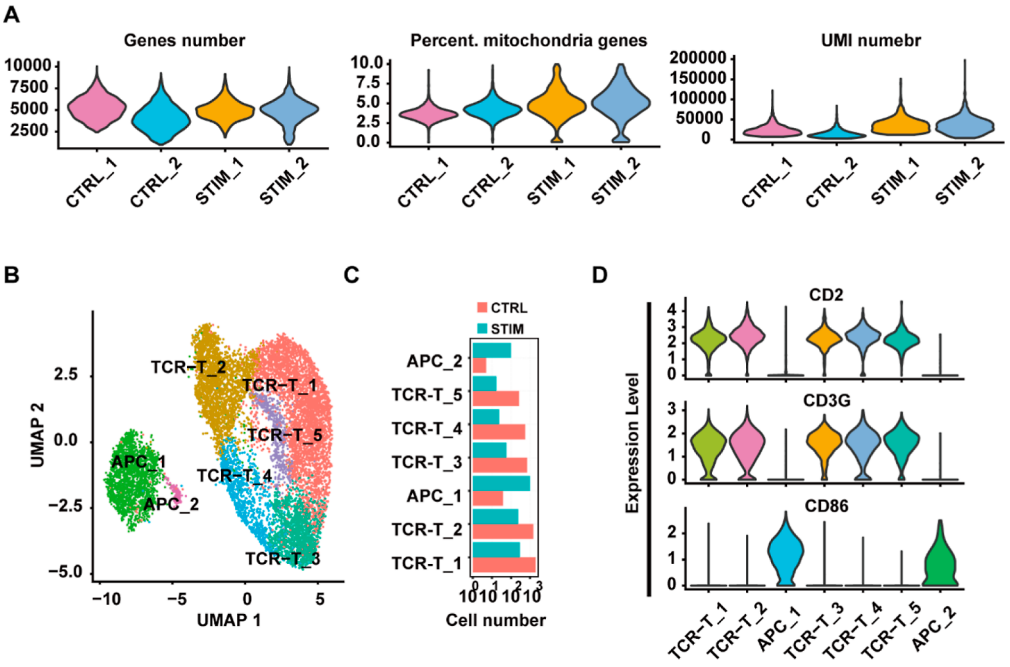

Figure 4. Qualification and classification of sorted cells by RNA sequencing. (A) Distribution of the gene number, percentage of mitochondria genes, and UMI number per cell for each sample. (B) UMAP of single cells clustered by gene expression. (C) Number of control and stimulated cells in each cluster. (D) Expression of classification markers in each cluster.

https://doi.org/10.1021/acs.analchem.1c03678
Anal. Chem. XXXX, XXX, XXX−XXX

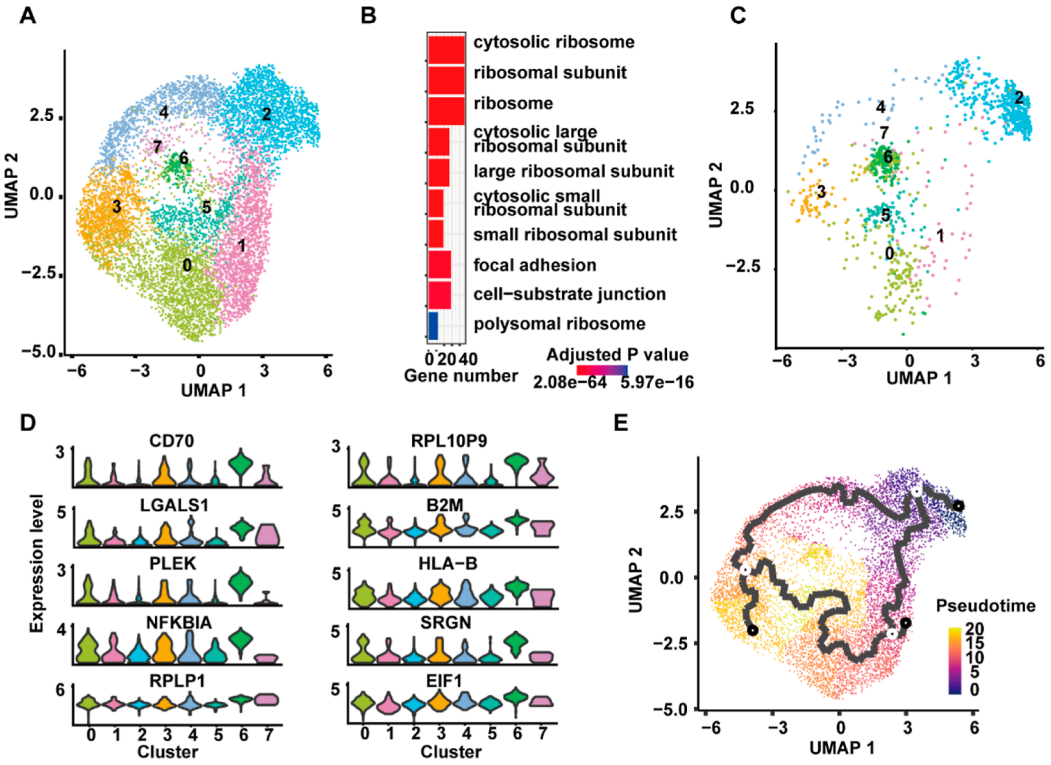

Figure 5. Heterogeneity of antigen-specific TCR-T cells. (A) UMAP of all TCR-T cells from stimulated and control samples. (B) GO analyses of DEGs of TCR-T cells from sorted droplets as compared with control cells. The top 10 signaling pathways ranked using the adjusted *P* values are shown. (C) UMAP of TCR-T cells from sorted droplets. (D) DEGs of TCR-T cells from cluster 6 as compared with other TCR-T cells from sorted droplets. (E) Trajectory analysis of cells.

within droplets.[39] Cells in droplets can float out of the center or focal plane of the laser spot, which induces variations in the signal received by the PMT. Thus, consistent cell positioning within the droplet[40] or applying multi-color bead-based normalization in droplets[41] can potentially improve the accuracy.

Single-cell RNA-sequencing. scRNA-seq on the functional TCR-T cells provides genetic information on the TCR−pMHC interactions, which could facilitate the design of ACTs. To further validate our platform and demonstrate that our platform is compatible with downstream genetic analysis, we performed scRNA-seq on the sorted TCR-T cells. Here, two samples of over 6000 cells were recovered from droplets (termed "STIM") and utilized for scRNA-seq. TCR-T cells without stimulation served as controls (termed "CTRL"). After alignment and error correction, 1581 and 2262 cells were recovered from two stimulated samples, respectively. 3036 and 4981 cells were detected from TCR-T cells of two control samples, respectively (Figure S9A). For both stimulated and control samples, mean genes per cell were between 4000 and 5000, UMI per cell was more than 10,000, and mean percentage of mitochondria genes per cell was 3.5−5% (Figure 4A). As comparisons, demos of the 3′ V3 kit for scRNA-seq from 10×, ddSEQ, and drop-seq achieved median 28006 UMIs/4776 genes, 10466 UMIs/3644 genes, and 8791 UMIs/3255 genes, respectively. These methods are common ones used for scRNA-seq. Therefore, the cells recovered from droplets are suitable for scRNA-seq and can achieve data with a high quality.[42,43]

RNA expression matrixes of two stimulated samples and two control samples were integrated using Seurat software. With a dimensionality reduction by the KNN graph and UMAP, cells were grouped into seven clusters (Figure 4B). Five clusters were gathered on the right-hand side, and two were on the left-hand side. Cells on the right-hand side were derived from stimulated and control samples, and these two groups mixed well (Figure S9B). In contrast, almost all cells (97.2%) on the left-hand side were from stimulated samples (Figure 4C). Because control samples had TCR-T cells only, cells on left-hand side might be APCs. Furthermore, right-hand side clusters highly expressed CD2 and CD3G, while left-hand side ones highly expressed CD86 (Figure 4D), confirming that APCs and TCR-T cells were discriminated completely. Captured cells could be stressed and damaged during the process including cell encapsulation, incubation, sorting, and library generation for scRNA-seq. The transcriptome of these low-quality cells is skewed, thus leading to misinterpretation of the data.[44] Setting arbitrary thresholds is a common approach to filter out low-quality cells (with genes < 1000, UMI < 1000, and/or increased percentage of mitochondria genes > 10% detected by scRNA-seq[45]), but it will only capture one part of the entire landscape of low-quality cells. Therefore, maintaining cell quality during the process is critical to perform scRNA-seq with good quality. According to results in bulk assay (Figure 2), a long-time stimulation with APCs facilitated GFP expression. To maintain cell status, we incubated cells in droplets for 6 h. Additionally, high-throughput sorting was another design to maintain cell viability.[46,47] Furthermore, a good cell status was confirmed from the scRNA-seq results, where the gene number, UMI number, and percentage of mitochondria genes per cell met the requirements for following analyses.[48]

After that, we removed APCs to avoid their influence on data integration and performed integration and clustering

https://doi.org/10.1021/acs.analchem.1c03678
Anal. Chem. XXXX, XXX, XXX−XXX

again. Eight clusters were presented by UMAP, and most cells from stimulated and control group samples were merged together, confirming the successful integration and heterogeneity of TCR-T cells (Figure 5A). Gene ontology (GO) analyses shown that ribosome-related genes were upregulated in cells of stimulated samples (Figure 5B), indicating the increased metabolism of activated TCR-T cells. Interestingly, cells from cluster 6 were derived from stimulated samples only (Figure 5C). GO analyses performed in TCR-T cells from stimulated samples showed that enriched genes of cluster 6 were cell proliferation-related (Figure 5D), suggesting that a part of TCR-T cells was more responsive to the stimulation via TCR than others. This hypothesis was further supported by the trajectory analysis, in which cells from cluster 6 had the largest distance from other clusters (Figure 5E). According to the DEGs listed in the Supporting Table, broad perturbations were shown in RNA expressions of stimulated TCR-T cells. In total, 878 DEGs had p values < 0.05 after being adjusted by the FDR method. GO analysis based on DEGs suggested that genes involved in functions of ribosomes were affected by TCR signaling largely. Among these DEGs, the expression of *HSPA6*, *HSPA1B*, *TRIB3*, and *IER3* was upregulated in stimulated cells with over 20%, and *CENPE* and *SYNE2* were downregulated by over 20%. *HSPA6* and *HSPA1B* were reported to be upregulated in the "TCR signaling pathway" defined by the KEGG database,[49] *TRIB3* and *IER3* were involved in the NF-κB pathway,[50,51] and *CENPE* was essential in maintaining microtubule capture,[52] suggesting broad alterations of survival and metabolism signaling in stimulated TCR-T cells. Because the activation and initiation of T cells requires orchestrated changes in cytokine, survival, proliferation, and metabolism signaling pathways,[53] our method potentially provides mechanistic data underlying the activation of T cells. Additionally, the fold change of DEGs in our study was less than that in other studies performed on primary cells. Partly, the count of APCs in droplets is far less than that in bulk assays, suggesting that the stimulation strength on TCR-T should be weaker. Additionally, we will develop our method by building a reporter system in primary T cells,[54] which should unveil the mechanism underlying the activation of real T cells.

Thus, the platform was well compatible with scRNA-seq, and the transcriptome information recovered from the scRNA-seq could precisely annotate cell status. Importantly, the development of TCR-T immunotherapy targeting neoantigens urgently seeks a high-throughput strategy for functionally screening TCRs for multiple neoantigens in parallel, and a combination of our platform and scRNA-seq could potentially meet this demand. An impressive development of multimer-MHC techniques is the employment of the DNA barcodes and scRNA-seq,[17] which overcomes the bottleneck of throughput. This strategy suggests that adding omics data to barcode antigens can also record messages of antigens to DNA sequences. Thus, instead of running our platform and scRNA-seq sequentially, we could potentially seamlessly integrate our platform with scRNA-seq in future.

The method developed in our study aims to identify TCRs with functions of recognizing pMHC and transducing signaling from TCR to downstream pathways. However, a triggering role of TCRs can only initiate the downstream signaling pathway and not decide the cell cytotoxicity. Cell status and helper signaling are primary factors to decide whether cellular cytotoxicity can be elicited, so the TCRs screened out might not be effective TCRs to eliminate the cancer cells in patients.

CONCLUSIONS

In summary, we developed a platform combining the cellular reporter system and fluorescence-activated droplet technique to achieve function-based high-throughput screening of tumor antigen-specific TCRs on a single-cell level. This strategy overcomes the weak correlation between function and TCR-pMHC affinity and the inefficient production presented by affinity-based methods. The new platform can screen millions of droplets per hour and sort target TCR-T cells in seconds with high accuracy. Therefore, our strategy shows a strong potential to address the shortcomings of traditional methods. Moreover, the strategy of combining with scRNA-seq will help unveil the molecular mechanism of TCR-pMHC recognition and promote scientific and clinical research. Importantly, scale-up of this platform would allow for more applications in the future.

ASSOCIATED CONTENT

Supporting Information

The Supporting Information is available free of charge at https://pubs.acs.org/doi/10.1021/acs.analchem.1c03678.

Droplet demulsification, details of scRNA-seq, microscope imaging, cell staining for FACS, software of droplet sorting, unsupervised clustering, DEG analysis, GO enrichment and trajectory analysis, design of microfluidic chips, stability study of chip I, distribution statistics of cells in droplets, generation of TCR-T cells, flow cytometry for identifying GFP-positive TCR-T cells, kinetics of GFP expression in TCR-T cells after anti-CD3 and anti-CD28 antibody stimulation, viability of TCR-T cells cultured in droplets, GFP expression of TCR-T cells stimulated by APC(s), and integration of single-cell RNA data (PDF)

Differently expressed genes between stimulated and unstimulated TCR-T cells (XLSX)

AUTHOR INFORMATION

Corresponding Authors

Zida Li − *Department of Biomedical Engineering, School of Medicine, Shenzhen University, Shenzhen 518060, China; Guangdong Key Laboratory for Biomedical Measurements and Ultrasound Imaging, Department of Biomedical Engineering, School of Medicine, Shenzhen University, Shenzhen 518060, China;* orcid.org/0000-0002-1353-9414; Email: zidali@szu.edu.cn

Longqi Liu − *BGI-Shenzhen, Shenzhen 518083, China; Shenzhen Bay Laboratory, Shenzhen 518000, China;* Email: liulongqi@genomics.cn

Ya Liu − *BGI-Shenzhen, Shenzhen 518083, China; Shenzhen Key Laboratory of Single-Cell Omics, BGI-Shenzhen, Shenzhen 518100, China;* orcid.org/0000-0002-3936-1685; Email: liuya1@genomics.cn

Authors

Shiyu Wang − *BGI-Shenzhen, Shenzhen 518083, China; College of Life Sciences, University of Chinese Academy of Sciences, Beijing 100049, China*

Yang Liu − *BGI-Shenzhen, Shenzhen 518083, China*

Yijian Li − *BGI-Shenzhen, Shenzhen 518083, China; College of Life Sciences, University of Chinese Academy of Sciences, Beijing 100049, China*

https://doi.org/10.1021/acs.analchem.1c03678
Anal. Chem. XXXX, XXX, XXX−XXX

Menghua Lv − *BGI-Shenzhen, Shenzhen 518083, China; College of Life Sciences, University of Chinese Academy of Sciences, Beijing 100049, China*
Kai Gao − *BGI-Shenzhen, Shenzhen 518083, China; College of Life Sciences, University of Chinese Academy of Sciences, Beijing 100049, China*
Ying He − *Department of Gynaecological Oncology, Cancer Hospital Chinese Academy of Medical Sciences, Shenzhen Center, Shenzhen 518116, China*
Wenbo Wei − *Department of Biomedical Engineering, School of Medicine, Shenzhen University, Shenzhen 518060, China; The First Affiliated Hospital of Shenzhen University, Shenzhen Second People's Hospital, Shenzhen 518035, China*
Yonggang Zhu − *School of Mechanical Engineering and Automation, Harbin Institute of Technology, Shenzhen 518055, China*
Xuan Dong − *BGI-Shenzhen, Shenzhen 518083, China*
Xun Xu − *BGI-Shenzhen, Shenzhen 518083, China; Guangdong Provincial Key Laboratory of Genome Read and Write, BGI-Shenzhen, Shenzhen 518120, China*

Complete contact information is available at: https://pubs.acs.org/10.1021/acs.analchem.1c03678

Author Contributions

[††]S.Y.-W and Y.-L. contributed equally to this work.

Notes

The authors declare no competing financial interest.

■ ACKNOWLEDGMENTS

We acknowledge financial supports from the China National GeneBank, the Shenzhen Key Laboratory of Single-Cell Omics (ZDSYS20190902093613831), the Shenzhen Basic Research Project for Excellent Young Scholars (no. 2020251518), the Guangdong Provincial Key Laboratory of Genome Read and Write (no. 2017B030301011), the China Postdoctoral Science Foundation (no.2021M692212), the National Natural Science Foundation of China (no. 31901072), and the Natural Science Foundation of Guangdong Province (2019A1515012010).

■ REFERENCES

(1) Magalhaes, I.; Carvalho-Queiroz, C.; Hartana, C. A.; Kaiser, A.; Lukic, A.; Mints, M.; Nilsson, O.; Grönlund, H.; Mattsson, J.; Berglund, S. *Expert Opin. Biol. Ther.* **2019**, *19*, 811−827.
(2) Rosenberg, S. A.; Yannelli, J. R.; Yang, J. C.; Topalian, S. L.; Schwartzentruber, D. J.; Weber, J. S.; Parkinson, D. R.; Seipp, C. A.; Einhorn, J. H.; White, D. E. *J. Natl. Cancer Inst.* **1994**, *86*, 1159−1166.
(3) Dudley, M. E.; Gross, C. A.; Somerville, R. P. T.; Hong, Y.; Schaub, N. P.; Rosati, S. F.; White, D. E.; Nathan, D.; Restifo, N. P.; Steinberg, S. M.; Wunderlich, J. R.; Kammula, U. S.; Sherry, R. M.; Yang, J. C.; Phan, G. Q.; Hughes, M. S.; Laurencot, C. M.; Rosenberg, S. A. *J. Clin. Oncol.* **2013**, *31*, 2152−2159.
(4) Goff, S. L.; Dudley, M. E.; Citrin, D. E.; Somerville, R. P.; Wunderlich, J. R.; Danforth, D. N.; Zlott, D. A.; Yang, J. C.; Sherry, R. M.; Kammula, U. S.; Klebanoff, C. A.; Hughes, M. S.; Restifo, N. P.; Langhan, M. M.; Shelton, T. E.; Lu, L.; Kwong, M. L. M.; Ilyas, S.; Klemen, N. D.; Payabyab, E. C.; et al. *J. Clin. Oncol.* **2016**, *34*, 2389−2397.
(5) Morgan, R. A.; Dudley, M. E.; Wunderlich, J. R.; Hughes, M. S.; Yang, J. C.; Sherry, R. M.; Royal, R. E.; Topalian, S. L.; Kammula, U. S.; Restifo, N. P.; Zheng, Z.; Nahvi, A.; de Vries, C. R.; Rogers-Freezer, L. J.; Mavroukakis, S. A.; Rosenberg, S. A. *Science* **2006**, *314*, 126−129.
(6) Lu, Y.-C.; Parker, L. L.; Lu, T.; Zheng, Z.; Toomey, M. A.; White, D. E.; Yao, X.; Li, Y. F.; Robbins, P. F.; Feldman, S. A.; van der Bruggen, P.; Klebanoff, C. A.; Goff, S. L.; Sherry, R. M.; Kammula, U. S.; Yang, J. C.; Rosenberg, S. A. *J. Clin. Oncol.* **2017**, *35*, 3322−3329.
(7) Kochenderfer, J. N.; Dudley, M. E.; Feldman, S. A.; Wilson, W. H.; Spaner, D. E.; Maric, I.; Stetler-Stevenson, M.; Phan, G. Q.; Hughes, M. S.; Sherry, R. M.; Yang, J. C.; Kammula, U. S.; Devillier, L.; Carpenter, R.; Nathan, D.-A. N.; Morgan, R. A.; Laurencot, C.; Rosenberg, S. A. *Blood* **2012**, *119*, 2709−2720.
(8) Jacoby, E.; Shahani, S. A.; Shah, N. N. *Immunol. Rev.* **2019**, *290*, 39−59.
(9) Zhao, L.; Cao, Y. *Front. Immunol.* **2019**, *10*, 02250.
(10) Wang, Z.; Han, W. *Biomark Res.* **2018**, *6*, 4.
(11) Harris, D. T.; Kranz, D. M. *Trends Pharmacol. Sci.* **2016**, *37*, 220−230.
(12) Brameshuber, M.; Kellner, F.; Rossboth, B. K.; Ta, H.; Alge, K.; Sevcsik, E.; Göhring, J.; Axmann, M.; Baumgart, F.; Gascoigne, N. R. J.; Davis, S. J.; Stockinger, H.; Schütz, G. J.; Huppa, J. B. *Nat. Immunol.* **2018**, *19*, 487−496.
(13) Soto, C.; Bombardi, R. G.; Kozhevnikov, M.; Sinkovits, R. S.; Chen, E. C.; Branchizio, A.; Kose, N.; Day, S. B.; Pilkinton, M.; Gujral, M.; Mallal, S.; Crowe, J. E., Jr. *Cell Rep.* **2020**, *32*, 107882.
(14) Gálvez, J.; Gálvez, J. J.; García-Peñarrubia, P. *Front. Immunol.* **2019**, *10*, 349.
(15) Campillo-Davo, D.; Flumens, D.; Lion, E. *Cells* **2020**, *9*, 1720.
(16) Sibener, L. V.; Fernandes, R. A.; Kolawole, E. M.; Carbone, C. B.; Liu, F.; McAffee, D.; Birnbaum, M. E.; Yang, X.; Su, L. F.; Yu, W.; Dong, S.; Gee, M. H.; Jude, K. M.; Davis, M. M.; Groves, J. T.; Goddard, W. A.; Heath, J. R.; Evavold, B. D.; Vale, R. D.; Garcia, K. C. *Cell* **2018**, *174*, 672−687.
(17) Bentzen, A. K.; Marquard, A. M.; Lyngaa, R.; Saini, S. K.; Ramskov, S.; Donia, M.; Such, L.; Furness, A. J. S.; McGranahan, N.; Rosenthal, R.; Straten, P. T.; Szallasi, Z.; Svane, I. M.; Swanton, C.; Quezada, S. A.; Jakobsen, S. N.; Eklund, A. C.; Hadrup, S. R. *Nat. Biotechnol.* **2016**, *34*, 1037−1045.
(18) Altman, J. D.; Moss, P. A. H.; Goulder, P. J. R.; Barouch, D. H.; McHeyzer-Williams, M. G.; Bell, J. I.; McMichael, A. J.; Davis, M. M. *Science* **1996**, *274*, 94−96.
(19) Klenerman, P.; Cerundolo, V.; Dunbar, P. R. *Nat. Rev. Immunol.* **2002**, *2*, 263−272.
(20) Newell, E. W.; Klein, L. O.; Yu, W.; Davis, M. M. *Nat. Methods* **2009**, *6*, 497−499.
(21) Zhang, S.-Q.; Ma, K.-Y.; Schonnesen, A. A.; Zhang, M.; He, C.; Sun, E.; Williams, C. M.; Jia, W.; Jiang, N. *Nat. Biotechnol.* **2018**, *36*, 1156−1159.
(22) Joglekar, A. V.; Li, G. *Nat. Methods* **2021**, *18*, 873−880.
(23) Hooijberg, E.; Bakker, A. Q.; Ruizendaal, J. J.; Spits, H. *Blood* **2000**, *96*, 459−466.
(24) Huang, H.; Wang, C.; Rubelt, F.; Scriba, T. J.; Davis, M. M. *Nat. Biotechnol.* **2020**, *38*, 1194−1202.
(25) Hwang, J.-R.; Byeon, Y.; Kim, D.; Park, S.-G. *Exp. Mol. Med.* **2020**, *52*, 750−761.
(26) Kisielow, J.; Obermair, F.-J.; Kopf, M. *Nat. Immunol.* **2019**, *20*, 652−662.
(27) Welsh, R. M.; Che, J. W.; Brehm, M. A.; Selin, L. K. *Immunol. Rev.* **2010**, *235*, 244−266.
(28) Segaliny, A. I.; Li, G.; Kong, L.; Ren, C.; Chen, X.; Wang, J. K.; Baltimore, D.; Wu, G.; Zhao, W. *Lab Chip* **2018**, *18*, 3733−3749.
(29) Klein-Hessling, S.; Muhammad, K.; Klein, M.; Pusch, T.; Rudolf, R.; Flöter, J.; Qureischi, M.; Beilhack, A.; Vaeth, M.; Kummerow, C.; Backes, C.; Schoppmeyer, R.; Hahn, U.; Hoth, M.; Bopp, T.; Berberich-Siebelt, F.; Patra, A.; Avots, A.; Müller, N.; Schulze, A.; et al. *Nat. Comm.* **2017**, *8*, 511.
(30) Liu, C.; Wu, T.; Fan, F.; Liu, Y.; Wu, L.; Junkin, M.; Wang, Z.; Yu, Y.; Wang, W.; Wei, W.; Yuan, Y.; Wang, M.; Cheng, M.; Wei, X.; Xu, J.; Shi, Q.; Liu, S.; Chen, A.; Wang, O.; Ni, M.; et al. *bioRxiv* **2019**, 818450.
(31) Guo, X.; Chen, F.; Gao, F.; Li, L.; Liu, K.; You, L.; Hua, C.; Yang, F.; Liu, W.; Peng, C.; Wang, L.; Yang, X.; Zhou, F.; Tong, J.;

Cai, J.; Li, Z.; Wan, B.; Zhang, L.; Yang, T.; Zhang, M.; et al. *Database* **2020**, baaa055.
(32) Chen, F. Z.; You, L. J.; Yang, F.; Wang, L. N.; Guo, X. Q.; Gao, F.; Hua, C.; Tan, C.; Fang, L.; Shan, R. Q.; Zeng, W. J.; Wang, B.; Wang, R.; Xu, X.; Wei, X. F. *Yi Chuan* **2020**, *42*, 799−809.
(33) Cohen, C. J.; Zhao, Y.; Zheng, Z.; Rosenberg, S. A.; Morgan, R. A. *Cancer Res.* **2006**, *66*, 8878−8886.
(34) Artyomov, M. N.; Lis, M.; Devadas, S.; Davis, M. M.; Chakraborty, A. K. *Proc. Natl. Acad. Sci.* **2010**, *107*, 16916−16921.
(35) Morimoto, S.; Fujiki, F.; Kondo, K.; Nakajima, H.; Kobayashi, Y.; Inatome, M.; Aoyama, N.; Nishida, Y.; Tsuboi, A.; Oka, Y.; Nishida, S.; Nakata, J.; Hosen, N.; Oji, Y.; Sugiyama, H. *Oncotarget* **2018**, *9*, 34132−34141.
(36) Vavouri, T.; Semple, J. I.; Garcia-Verdugo, R.; Lehner, B. *Cell* **2009**, *138*, 198−208.
(37) Morancho, B.; Minguillón, J.; Molkentin, J. D.; López-Rodríguez, C.; Aramburu, J. *BMC Mol. Biol.* **2008**, *9*, 13.
(38) Kleinovink, J. W.; Mezzanotte, L.; Zambito, G.; Fransen, M. F.; Cruz, L. J.; Verbeek, J. S.; Chan, A.; Ossendorp, F.; Löwik, C. *Front. Immunol.* **2019**, *9*, 03097.
(39) Cossarizza, A.; Chang, H. D.; Radbruch, A.; Akdis, M.; Andrä, I.; Annunziato, F.; Bacher, P.; Barnaba, V.; Battistini, L.; Bauer, W. M.; Baumgart, S.; Becher, B.; Beisker, W.; Berek, C.; Blanco, A.; Borsellino, G.; Boulais, P. E.; Brinkman, R. R.; Büscher, M.; Busch, D. H.; et al. *Eur. J. Immunol.* **2017**, *47*, 1584−1797.
(40) Eyer, K.; Doineau, R. C. L.; Castrillon, C. E.; Briseño-Roa, L.; Menrath, V.; Mottet, G.; England, P.; Godina, A.; Brient-Litzler, E.; Nizak, C.; Jensen, A.; Griffiths, A. D.; Bibette, J.; Bruhns, P.; Baudry, J. *Nat. Biotechnol.* **2017**, *35*, 977−982.
(41) Shembekar, N.; Hu, H.; Eustace, D.; Merten, C. A. *Cell Rep.* **2018**, *22*, 2206−2215.
(42) Yamawaki, T. M.; Lu, D. R.; Ellwanger, D. C.; Bhatt, D.; Manzanillo, P.; Arias, V.; Zhou, H.; Yoon, O. K.; Homann, O.; Wang, S.; Li, C.-M. *BMC Genomics* **2021**, *22*, 66.
(43) Macosko, E. Z.; Basu, A.; Satija, R.; Nemesh, J.; Shekhar, K.; Goldman, M.; Tirosh, I.; Bialas, A. R.; Kamitaki, N.; Martersteck, E. M.; Trombetta, J. J.; Weitz, D. A.; Sanes, J. R.; Shalek, A. K.; Regev, A.; McCarroll, S. A. *Cell* **2015**, *161*, 1202−1214.
(44) Ilicic, T.; Kim, J. K.; Kolodziejczyk, A. A.; Bagger, F. O.; McCarthy, D. J.; Marioni, J. C.; Teichmann, S. A. *Genome Biol.* **2016**, *17*, 29.
(45) Mereu, E.; Lafzi, A.; Moutinho, C.; Ziegenhain, C.; McCarthy, D. J.; Álvarez-Varela, A.; Batlle, E.; Sagar; Grün, D.; Lau, J. K.; Boutet, S. C.; Sanada, C.; Ooi, A.; Jones, R. C.; Kaihara, K.; Brampton, C.; Talaga, Y.; Sasagawa, Y.; Tanaka, K.; Hayashi, T.; et al. *Nat. Biotechnol.* **2020**, *38*, 747−755.
(46) Xi, H.-D.; Zheng, H.; Guo, W.; Gañán-Calvo, A. M.; Ai, Y.; Tsao, C.-W.; Zhou, J.; Li, W.; Huang, Y.; Nguyen, N.-T.; Tan, S. H. *Lab Chip* **2017**, *17*, 751−771.
(47) Frenzel, D.; Merten, C. A. *Lab Chip* **2017**, *17*, 1024−1030.
(48) Hao, Y.; Hao, S.; Andersen-Nissen, E.; Mauck, W. M.; Zheng, S.; Butler, A.; Lee, M. J.; Wilk, A. J.; Darby, C.; Zager, M.; Hoffman, P.; Stoeckius, M.; Papalexi, E.; Mimitou, E. P.; Jain, J.; Srivastava, A.; Stuart, T.; Fleming, L. M.; Yeung, B.; Rogers, A. J.; et al. *Cell* **2021**, *184*, 3573−3587.
(49) Chiricosta, L.; Gugliandolo, A.; Bramanti, P.; Mazzon, E. *Genes* **2020**, *11*, 615.
(50) Yu, Y.; Qiu, L.; Guo, J.; Yang, D.; Qu, L.; Yu, J.; Zhan, F.; Xue, M.; Zhong, M. *Mol. Oral Microbiol.* **2015**, *30*, 295−306.
(51) Arlt, A.; Schäfer, H. *Eur. J. Cell Biol.* **2011**, *90*, 545−552.
(52) Weaver, B. A. A.; Bonday, Z. Q.; Putkey, F. R.; Kops, G. J. P. L.; Silk, A. D.; Cleveland, D. W. *J. Cell Biol.* **2003**, *162*, 551−563.
(53) Pennock, N. D.; White, J. T.; Cross, E. W.; Cheney, E. E.; Tamburini, B. A.; Kedl, R. M. *Adv. Physiol. Educ.* **2013**, *37*, 273−283.
(54) Bartelt, R. R.; Cruz-Orcutt, N.; Collins, M.; Houtman, J. C. D. *PloS one* **2009**, *4*, No. e5430.

https://doi.org/10.1021/acs.analchem.1c03678
Anal. Chem. XXXX, XXX, XXX−XXX